ROYAL SOCIETY
OF CHEMISTRY

PAPER

Check for updates

Sustainable removal of malachite green using cellulose extracted from waste bamboo culm sheath

Diptiranjan Behera,†[a] Priyanka P. Mishra,†[a] Shruti S. Pattnaik,[a] Nigamananda Das, [iD] [ab] Jagadish Kumar [iD] [c] and Ajaya K. Behera [iD] *[ab]

The sustainable utilization of waste biomass for wastewater treatment aligns with the principles of green chemistry and the circular economy. In this study, cellulose was extracted from waste bamboo culm sheath (BCS) and evaluated as a renewable and reusable adsorbent for removing malachite green (MG) from aqueous solutions. Dynamic light scattering confirmed a cellulose size of 108 nm, while structural and morphological analyses were conducted using X-ray diffraction, field-emission scanning electron microscopy, FT-IR, and atomic force microscopy. The adsorption process was pH-dependent, with optimal removal of 92.8% MG (20 mg L^{-1}) within 120 minutes. Kinetic studies indicated pseudo-first-order behavior, and the Langmuir isotherm model estimated a maximum monolayer adsorption capacity of 111.11 mg g^{-1}. Reusability tests demonstrated over 80% removal efficiency up to four cycles, supporting its long-term application. This study presents an eco-friendly approach to wastewater remediation, demonstrating the potential of BCS-derived cellulose as a sustainable adsorbent for dye removal, contributing to responsible resource utilization and environmental protection.

Sustainability spotlight

The pursuit of sustainable water treatment solutions necessitates the development of eco-friendly and high-performance materials. This research addresses the urgent need for sustainable dye remediation by utilizing waste bamboo culm sheath (BCS) to produce cellulose, a renewable and biodegradable adsorbent. By valorizing an abundant agro-waste material, this study aligns with the principles of the circular economy while mitigating environmental pollution. The cellulose demonstrated high efficiency in removing hazardous malachite green (MG) dye, with excellent reusability, thereby reducing chemical waste and supporting responsible resource consumption. This innovative approach not only transforms waste biomass into a valuable adsorption material but also contributes to cleaner water systems and sustainable production practices. By integrating waste valorization with wastewater treatment, this research highlights the potential of green chemistry in advancing environmental sustainability.

1 Introduction

The rapid expansion of industrialization and technological advancements has intensified water pollution, posing a serious environmental and public health challenge. Industries such as textiles, leather, printing, paper, plastics, cosmetics, food processing, rubber, and petroleum release substantial amounts of organic pollutants, including synthetic dyes, into water bodies. Globally, over 7 million tons of approximately 10 000 industrial dyes are produced annually, with nearly 20% of these dyes being discharged as effluents.[1,2] These synthetic dyes, including malachite green (MG), are persistent pollutants, exhibiting toxic, mutagenic, and allergenic properties, even at low concentrations in water (<1 mg L^{-1}).[3,4] Malachite green, a triphenylmethane dye widely used in textiles, leather processing, distilleries, and aquaculture, is associated with severe health risks, including liver, kidney, and intestinal damage, while also being detrimental to aquatic and microbial life.[5,6] The complex molecular structure of synthetic dyes enhances their resistance to biodegradation, as they remain stable under exposure to light, heat, water, and chemical treatments.[7]

Several conventional treatment techniques, such as electrodialysis, reverse osmosis, ion exchange, ultrafiltration, and chemical precipitation, have been employed to combat dye pollution. However, these methods often suffer from high operational costs, energy consumption, partial removal efficiency, and secondary waste generation.[8,9] In contrast, adsorption has emerged as an efficient and economically viable alternative for dye removal due to its simple design, ease of

[a]*Department of Chemistry, Utkal University, Bhubaneswar, Odisha 751004, India. E-mail: ajayabehera@utkaluniversity.ac.in; Fax: +91 0674 2581850; Tel: +91 9938956715*

[b]*Centre for Advance Materials and Application, Utkal University, Bhubaneswar, Odisha 751004, India*

[c]*Department of Physics, Utkal University, Bhubaneswar, Odisha 751004, India*

† These authors contributed equally.

operation, cost-effectiveness, and ability to eliminate contaminants, even from highly diluted solutions.[10] Recent research efforts have focused on developing recyclable and sustainable adsorbents derived from renewable biomass to address water contamination challenges.

Cellulose, the most abundant biopolymer on earth, is a linear polysaccharide composed of β-D-glucose units linked via β-(1→4)-glycosidic bonds. It is an attractive natural alternative to synthetic polymers due to its renewable availability, non-toxicity, and biodegradability.[11] Extracted from diverse sources, including wood, grasses, and algae, cellulose finds applications in industries such as food, pharmaceuticals, paints, and textiles.[12] The emergence of nanocellulose, characterized by its exceptional mechanical properties, high surface area, and tunable functional groups, has opened new avenues for applications in nanocomposites and water remediation.[13] Its robust hydrogen-bonded network imparts mechanical strength, making it an ideal candidate for adsorptive applications. Bassyouni *et al.* synthesized nanocellulose/chitosan-based composites using nanocellulose from palm leaves, demonstrating high removal efficiency (91.5%) for direct blue 78 dye in textile wastewater.[14] Chauhan *et al.* fabricated spherical nanocellulose (SNC) from pine needles and functionalized it with methionine ester, achieving high adsorption capacities (94.8% for Hg^{2+} and 96.1% for Congo red dye).[15] Tan *et al.* developed biomass-derived adsorbents from passion fruit leaves for wastewater treatment, reporting a Langmuir monolayer capacity of 227.3 mg g^{-1} for AB113 and 666.7 mg g^{-1} for methylene blue (MB) dye, demonstrating cost-effectiveness comparable to commercial activated carbons.[16]

Bamboo-based biomass has gained significant attention as a renewable resource with promising applications in environmental sustainability. Bamboo culm sheath (BCS), an agricultural waste byproduct of *Dendrocalamus giganteus*, is traditionally used as natural soil fertilizer or as biofuel in rural communities. It is abundantly available in Asian countries such as China, India, Sri Lanka, and Bangladesh.[17] Comprising holocellulose (70.17%), acid-insoluble lignin (21.65%), acid-soluble lignin (1.72%), toluene–alcohol extract (2.66%), SiO_2 (1.50%), and ash (3.21%), BCS is an excellent source of cellulose with a high degree of functionalization, making it a promising candidate for adsorption applications.[17,18]

Although BCS-derived cellulose is rich in cellulose, its potential as an effective and sustainable adsorbent for dye removal has not been thoroughly investigated. This research seeks to address this gap by employing cellulose obtained from BCS as an environmentally friendly, economical, and reusable adsorbent to eliminate malachite green from water solutions. The innovation of this study lies in its emphasis on using an underutilized biomass resource for wastewater treatment, thereby adding to the expanding research on eco-friendly adsorbents. Moreover, since the extracted cellulose undergoes no additional chemical alterations, it serves as a lucrative and practical adsorbent compared to other modified cellulose-based materials reported in the literature. Furthermore, biosorbents often encounter issues such as limited adsorption capacity and prolonged contact times in the removal process, but cellulose derived from BCS effectively overcomes these drawbacks.[19,20] Ensuring sustainability through the recyclability and reuse of adsorbent materials is essential for achieving a zero-waste strategy. The adsorption performance was analysed with respect to pH, temperature variation, contact time, and MG concentration, with equilibrium and kinetic modelling providing insights into the adsorption mechanism. This study advances the development of sustainable materials for water purification and lays the foundation for future applications in dye and heavy metal removal, aligning with global sustainability goals.

2 Materials and methodology

2.1. Materials

Bamboo culm sheaths were obtained from the Utkal University campus, in Bhubaneswar, India. Chemicals like toluene (CAS no. 108-88-3, SRL, India), ethanol (CAS no. 64-17-5, Merck, India), KOH (CAS no. 1310-58-3, Finar, India), sodium perchlorate ($NaClO_4$, CAS no. 7601-89-0, Finar, India), acetic acid (CAS no. 64-19-07, Finar, India) and malachite green chloride (MG, CAS no. 569-64-2, ≥90%, Finar, India) were procured and used as such.

2.2. Extraction of cellulose from bamboo culm sheath (BCS)

To prepare the bamboo culm sheaths for use, they underwent a thorough cleaning process with warm water, repeated 3–4 times to remove dirt and other water-soluble substances. Afterward, they were dried at a temperature of 50 °C. The dried and purified sheaths were then crushed into a fine powder using a grinder and carefully sieved through a Tyler mesh. Following this, cellulose was extracted from this BCS powder through four steps. Initially, (i) Soxhlet extraction was employed to eliminate waxes, using a 2 : 1 (v/v) mixture of toluene to ethanol (EtOH) at 155 °C for 5 hours; then (ii) the solid material was separated and allowed to dry for 24 hours at 60 °C. In the next step, (iii) water-soluble lignin and polysaccharides were removed *via* treatment with deionized water, with the BCS immersed in a 1 : 25 (g : mL) ratio at 80 °C and 300 rpm for 4 hours. (iv) Vacuum filtration was used to isolate the solid material, which was then dried for 24 hours. The subsequent step involved the removal of insoluble lignin using a 3 wt% bleach solution of $NaClO_4$ (pH 3.6) at a 1 : 20 (g : mL) ratio with the BCS, followed by an acid treatment at 75 °C for 2 hours. Again, vacuum filtration was used, and the collected solid was washed until neutral before drying. Finally, a basic treatment with aqueous KOH (18 wt%) for 2 hours at room temperature was employed to eliminate hemicellulose and remaining lignin, resulting in pure cellulose. It was then filtered, rinsed with ethanol, neutralized with deionized water, and dried at 60 °C for 24 hours.[21,22] The yield of bamboo-extracted cellulose was found to be 77.8%. The extracted cellulose was milled using a planetary ball mill (NST_HM_O63, India), with 5 mm diameter agate balls. The milling was carried out at a rotation speed of 800 rpm for 60 minutes with a gap period of 5 minutes. The milled cellulose was then characterized using DLS, FESEM, and TEM to
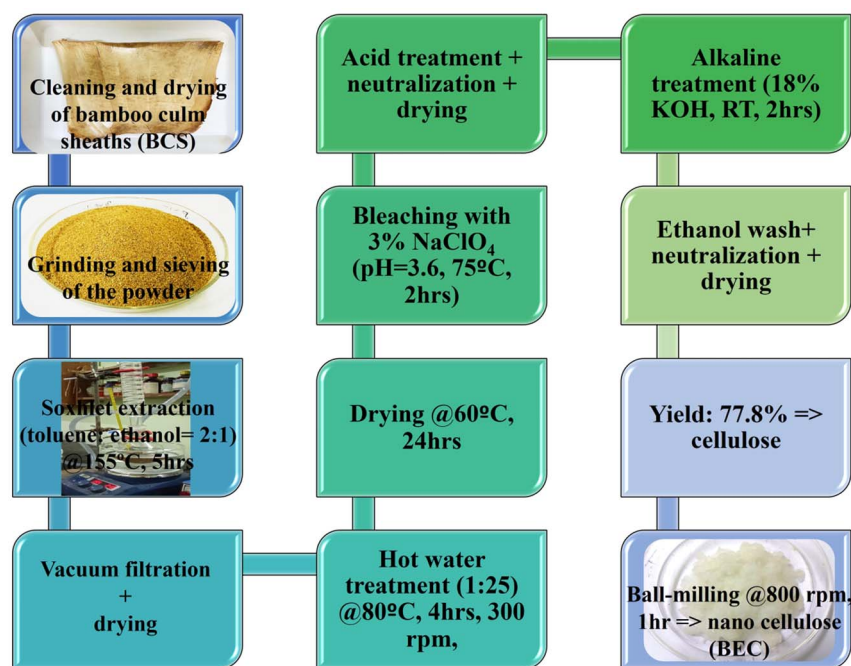
Fig. 1 Flowchart for the extraction of cellulose (BEC) from bamboo-culm-sheaths (BCSs).

confirm its nanoscale form.[23] The procedure for the extraction of cellulose (BEC) from bamboo cum sheath is shown in Fig. 1.

2.3. Characterization

The bamboo-extracted cellulose (BEC) was subjected to different characterization techniques to evaluate its structural backbone. Using a SHIMADZU, IRAffinity-1S spectrometer, Fourier transform infrared (FTIR) spectra were recorded between 400 and 4000 cm^{-1} with the KBr pellet method. The BEC sample was dispersed in deionized water and measured for particle size and zeta potential using a Zetasizer (Malvern Instruments Ltd, UK) with DTS 1060 plastic cells and DTS 1070 capillary cells. The point of zero charge (pH$_{pzc}$) for BEC was determined using techniques outlined by Bach *et al.*[24] The process involved adding BEC powder at a concentration of 1 g L^{-1} to a KCl solution (0.1 M) with pH values ranging from 3–11. This mixture was agitated for 10 min and then allowed to settle for over 24 h to achieve equilibrium before the final pH was measured. The results were visualized by plotting a graph that displayed the change in pH against the initial pH values. The surface morphology of the sample was examined using a Zeiss EVO field emission scanning electron microscope operated at 25 kV acceleration voltage and a high-resolution transmission electron microscope (HRTEM, Jeol Jem F200) operated at 200 kV. An MFP 3D Origin (Asylum Research AFM) atomic force microscope was used to obtain the 3D topographic image and surface roughness data of the sample. The measurement was performed in contact mode with a silicon nitride probe having a diameter of 10–20 nm. A 1 mm-thick BEC pellet was prepared before analysis and a scanning rate of 0.5 Hz was applied to obtain the AFM images. Furthermore, a thermogravimetric analysis plot was obtained by analyzing samples using a TG

analyzer (NETZSCH, STA 449F5, Jupiter) in an N$_2$ environment at a heating rate of 10 °C min^{-1} between 30 and 500 °C as the organic component present in the derived cellulose decompose within 500 °C. The BEC and BCS powder X-ray diffraction patterns were recorded using a Philips-PW 1800 diffractometer and CuK$_\alpha$ radiation with $\lambda = 1.54186$ Å. The crystallinity index of the BEC was calculated using the following eqn (1).

$$\text{Crystallinity index}(\%) = \frac{(I_{200} - I_{am})}{I_{200}} \times 100 \qquad (1)$$

where I_{200} is the intensity of the crystalline phase and I_{am} is the intensity of the amorphous phase.

### 2.4. Theoretical analysis using density functional theory (DFT)

DFT calculations were carried out through the ORCA 5.0 program using the hybrid B3LYP/g function with a def2/J basis set, to optimize the molecular geometry of MG, cellobiose (for BEC).[25] Their ground state geometry and HOMO and LUMO interactions are drawn by using Avogadro 1.2.0 software. The interaction energy between MG and cellobiose (E_{inter}) was calculated at the same basis set and level of theory through eqn (2).[26]

$$E_{inter} = E_{MG-cellobiose} - (E_{MG} + E_{cellobiose}) \qquad (2)$$

where $E_{MG-cellobiose}$, E_{MG}, and $E_{cellobiose}$ are the total energies of the MG–cellobiose complex, MG, and cellobiose unit.

2.5. Adsorption activity

2.5.1. Adsorbate preparation. This study investigated the removal of malachite green (MG) dye. For the preparation of the
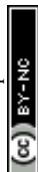
standard solution, the dye (0.5 g) was dispersed in 1.0 L of distilled water to prepare a standard solution of MG (500 mg L^{-1}) (3D image is shown in Fig. 3a). The solution sample was then diluted based on the initial MG dye concentrations of 20, 40, 60, 80, and 100 mg L^{-1}.

2.5.2. Dye adsorption study. The study examined several operational factors, including pH (from 2 to 8), dye concentration (ranging from 20 to 100 mg L^{-1}), contact time (0 to 120 min), and temperature (25 °C to 45 °C). In the batch adsorption experiment, the adsorbent was introduced into a 100 mL dye solution with specific pH levels, adjusted using HCl or NaOH. The mixture was agitated at 290 rpm in a thermostat bath shaker at ambient temperature (25 °C). Subsequently, the supernatant of the MG dye solution was collected and centrifuged. The dye absorbance was measured using a spectrophotometer λ_{max} = 620 nm to determine the initial concentration and equilibrium of the dyes. The sorption capacity of MG dye was calculated according to eqn (3).[22]

$$q_e = \frac{(A_0 - A_e)}{M} \times V \qquad (3)$$

where q_e is the equipoise sorption capability (mg g^{-1}); A_0 is the initial and A_e is the optimum concentrations of dye in the solution (mg L^{-1}); V is the total volume of the solution (mL) and M is the weight of adsorbent (g). The amount of dye adsorption was determined using eqn (4), where spectral analysis was performed on an Agilent UV-visible spectrophotometer (USA).[22]

$$\text{Dye removal}(\%) = \frac{(A_0 - A_t)}{A_0} \times 100 \qquad (4)$$

Under optimized conditions, adsorption kinetics, isotherms, and regeneration studies were investigated.

2.5.3. Adsorption isotherms. Adsorption capacity calculations and mechanism identification in adsorption system design often rely on isotherm models. In this research, the Langmuir and Freundlich isotherm models were examined. The linear and non-linear mathematical equations (eqn (5)–(8)) for these isotherm models are presented in Tables 2 and S1, respectively.

2.5.4. Adsorption kinetics. A kinetic study was conducted to investigate the adsorption behaviour of dye onto the extracted cellulose. The study examined pseudo-first-order and pseudo-second-order models to determine the controlling mechanism. The linear (Table 3, eqn (11) and (12)) and non-linear expressions of these kinetic models are derived from eqn (13) and (14) (presented in Fig. S1 and Table S2). Then the dye concentrations were monitored over time, and the collected data were plotted using various kinetic models to analyze the adsorption process.

2.5.5. Regeneration and reusability studies. To assess the potential for reuse of extracted cellulose, the adsorbents underwent a regeneration process using 70% v/v ethanol. After the adsorption process, the adsorbents were treated with ethanol solution for 5 minutes. Subsequently, they were rinsed and dried before being used in the next adsorption cycle. This process was repeated over five cycles, with the adsorption efficiency evaluated after each cycle.

3 Results and discussion

3.1. FTIR analysis

Fig. 2A depicts the FTIR analysis of the BEC and BCS, as well as BEC–MG interactions. FTIR analysis of the BCS and BEC was performed to investigate the structural changes that occur in the material following chemical treatment and to confirm that the resulting product is pure cellulose. Both exhibited comparable spectra, signifying that chemical methods used to isolate BEC from BCS did not change their chemical structure. A prominent band at 3332 cm^{-1} for BEC is associated with the stretching vibration of O–H groups. The peak in BEC was intense and sharper compared to BCS, where it appeared less intense and broader. This difference is due to the higher crystallinity of BEC, which exhibits well-defined molecular vibrations, leading to sharper and more intense peaks. In contrast, the amorphous structure of BCS lacked long-range molecular order, resulting in a broader peak in the FTIR spectra.[27] The characteristic band at 2899 cm^{-1} is attributed to symmetric C–H vibrations.[28] Intense absorption from adsorbed water was detected at 1606 cm^{-1}. The wide band at 1683 cm^{-1}, corresponding to the vibrations of the acetyl groups and ester linkages in hemicellulose and lignin present in the BCS, appeared sharper in the case of BEC, clearly indicating the reduction of hemicellulose and lignin in BEC.[29] The wide peak at 1041 cm^{-1} associated with the C–O–C pyranose ring vibration became
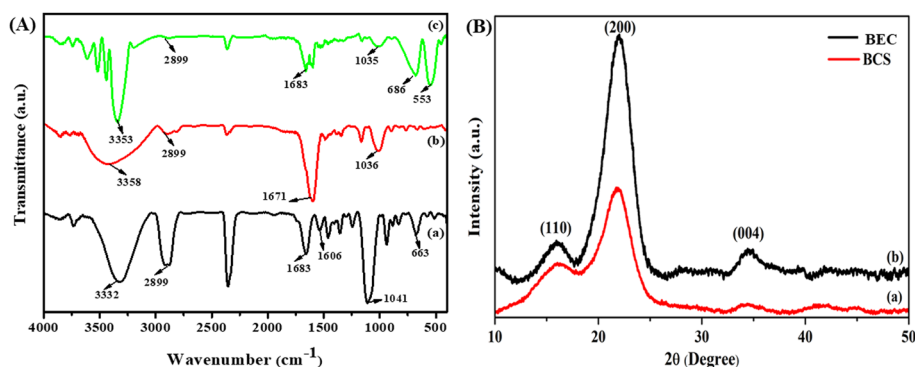

Fig. 2 (A) FTIR spectra of (a) BEC, (b) BCS, and (c) BEC–MG (after adsorption) and (B) XRD pattern of (a) BCS, and (b) BEC.

a sharper and narrower band, indicating the presence of more cellulose in the case of BEC.[30] Moreover, the peak at 663 cm^{-1} was associated with the C–OH out-of-plane bending mode found in BEC.[28] FTIR spectra also determined the qualitative changes in cellulose chemical functional groups before and after dye adsorption. The cellulose characteristics changed after adsorption, as evidenced by the emergence of new spectral peaks in cellulose. In the MG adsorbed spectrum, –OH stretching frequency shifts from 3332 cm^{-1} to 3353 cm^{-1} after the sorption process, signifying the coordination of –OH with MG. This shows that the adsorption occurred through bonding of the active site of cellulose with the active side of the dye.[31]

3.2. X-ray diffraction (XRD) analysis

The X-ray diffraction (XRD) analysis for both the natural BCS and the extracted cellulose are depicted in Fig. 2B. The crystallinity index was determined using eqn (1) and it was found to be 73.04% for BEC. The XRD patterns for both materials reveal three peaks at $2\theta = 16.3°$, $22.6°$, and $34.8°$, which correspond to the 110, 200, and 004 crystal planes, respectively. However, the peak intensities of the extracted cellulose were stronger than those of the natural bamboo culm sheath, which may be attributed to the selective removal of amorphous lignin and hemicellulose during sodium chlorite treatment of the bamboo culm sheath. The principal crystalline peak was observed at 22.6° with an intensity of 100%, indicating a crystallinity index of 73.04%, which is higher than the crystalline index of neat bamboo (25.08%).[32] The observed higher crystallinity index of BEC can be attributed to the formation of hydrogen bonds between the hydroxyl groups and the fibrillar surface of the BCS during the sodium chlorite treatment.

3.3. Theoretical analysis

This study uses quantum chemical computations based on conceptual density functional theory to evaluate the influence of

Table 1 Data interpretation from DFT calculations

Specimen	E_{HOMO} (eV)	E_{LUMO} (eV)	ΔE_{GAP} (eV)
MG	−4.456	−2.585	1.187
Cellobiose	−6.628	1.046	7.674

Specimen	Total energy after integration (eV)
MG	−39 760.81119
Cellobiose	−35 317.79224
MG–cellobiose	−75 078.62264
Total interaction energy (eV)	−0.01921

molecular structure on the adsorption process of MG molecules onto the surface of the adsorbent. The optimized molecular structures of MG and cellobiose, including their highest occupied molecular orbital (HOMO) and lowest unoccupied molecular orbital (LUMO), are illustrated in Fig. 3. The HOMO and LUMO orbitals are predominantly located on the MG particle and the oxygen atoms of the cellulose extracted from bamboo culm sheath (BCS), indicating that these areas likely serve as active sites for biosorption.[3] The effects of MG biosorption on the molecular properties of different components of cellobiose, along with the values of E_{HOMO}, E_{LUMO}, and ΔE_{GAP} for both MG and cellobiose, were assessed, with the results presented in Table 1. Generally, the total energy (E_{Tot}) of individual molecules may determine their stability and reactivity; a higher E_{Tot} value indicates a more stable molecule, while a lower E_{Tot} value suggests a greater tendency for adsorption.[26] E_{HOMO} generally reflects a molecule's ability to donate electrons, while E_{LUMO} indicates its capacity to accept electrons, which is related to its electron affinity. A higher E_{HOMO} value suggests a greater affinity of
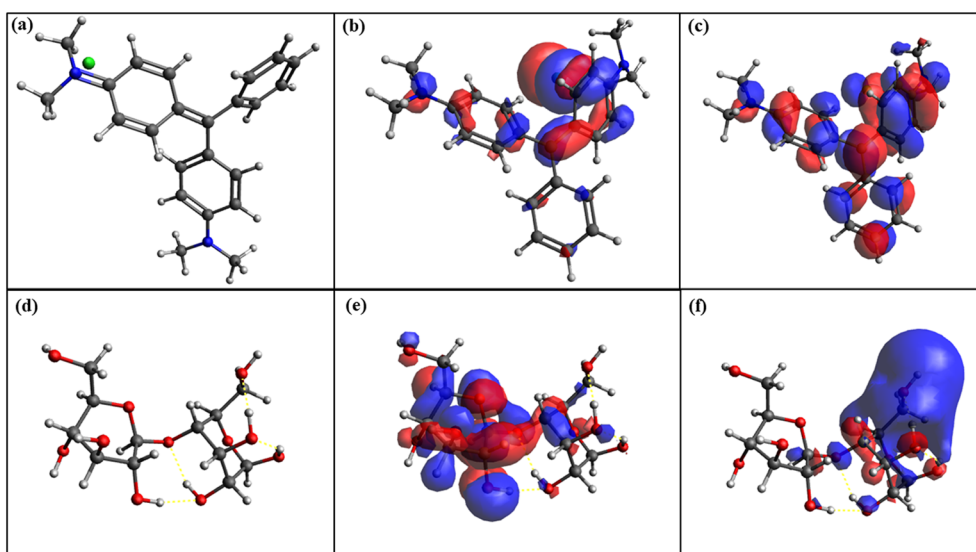

Fig. 3 Optimized molecular structure of (a) malachite green, and its (b) HOMO and (c) LUMO and (d) the optimized molecular structure of cellobiose, and its (e) HOMO and (f) LUMO.

electron transfer to an appropriate acceptor molecule, facilitating the adsorption of MG molecules onto the surface of cellobiose. Additionally, a smaller ΔE_{GAP} value indicates higher reactivity, enhancing the biosorption of MG onto cellobiose (BEC) and suggesting that the process is more stable.[3] Binding energy calculations further confirm the strong interaction between cellobiose and MG. The detailed adsorption phenomena of the dye have been mentioned in Section 3.8.7.

3.4. Thermal stability analysis *via* thermo-gravimetry

Application of the extracted cellulose for wastewater treatment requires knowledge of its performance under high-temperature conditions. This was evaluated using thermo-gravimetric results (TG and DTG curves) of the raw form of bamboo culm sheath and its extracted cellulose, as shown in Fig. 4A. In the temperature range of 222–378 °C, both BEC and BCS show a gradual thermal transition, basically related to the initial chain degradation of the cellulose. Also, a sharp loss in weight (almost 90%) was observed in this phase. The major reason behind this can be attributed to the pyrolysis of cellulose. The initial drop in the TG curves, up to 220 °C, represents the evaporation of excess moisture bound to the material. The degradation temperature confirms that the extracted cellulose has higher thermal stability as compared to BCS.[33] Additionally, the DTG curve approves the stability up to 282 °C and 298 °C, for BCS and BEC respectively, through the prominent peaks, hence indicating the same.

3.5. Dynamic light scattering (DLS) studies

Fig. 4B presents the Dynamic Light Scattering (DLS) measurements, showing that nearly all the BEC particles exhibit an average hydrodynamic diameter of 108 nm. This finding confirms the presence of consistently small particle sizes across the sample, indicating that BEC is well-dispersed in the nano-scale range. The uniformity in particle size distribution further supports the potential for BEC to enhance the surface area for adsorption.[32]

3.6. Morphological analysis

The surface structures of the samples were examined using a field emission scanning electron microscope (FESEM). Fig. 5a and b displays the external morphology of BCS and BEC, respectively. BCS exhibited a porous structure,[3] while BEC showed spherical, flat-bowl-like formations. These smooth yet uneven surfaces of BEC likely created spaces for the accumulation of MG molecules, contributing to their higher adsorption efficiency in aqueous solutions.[34] These facts are further supported by the FE-SEM image of BEC after dye adsorption, shown in Fig. 5c, which shows a roughened surface due to the adsorption of MG onto the cellulose. The elemental composition, confirmed by EDAX spectra (Fig. 5d), indicated the presence of carbon (C) and oxygen (O) in the BEC particles. HRTEM images (Fig. 5e and f) further demonstrated spherical particles with sizes ranging from 30 to 40 nm, with both crystalline (CR) and amorphous (AR) regions coexisting in varying orientations within the BEC particles.[35] The existence of both CR and AR is also verified from XRD images as shown in Fig. 2B.

3.7. Atomic force microscopy (AFM) analysis

The nano-scale morphology of BEC was additionally confirmed using AFM and is presented in Fig. 6. The obtained root mean square surface roughness of the BEC sample was about 90 nm, which adheres to the findings of the microscopic analysis conducted before. The AFM images also represent the amorphous and crystalline areas of the BEC *via* the shadier and light areas, respectively. The dominance of the light-colored area marks the presence of the majorly crystalline nature of BEC. This is also coherent with the data obtained through the XRD patterns.[32] Fig. 6c represents the roughness profile along the horizontal line drawn from the AFM image of BEC.

3.8. Adsorption studies

3.8.1. Effect of pH. The surface charge of the sorbent, the disintegration of functional molecules at the sorbent active sites, and the chemical characteristics of the dye mixture are all
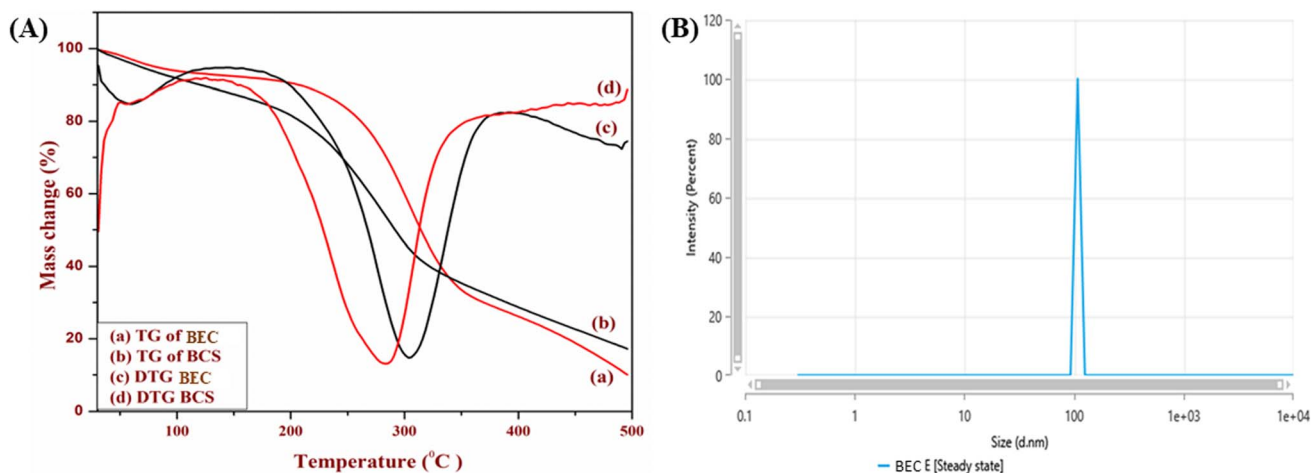

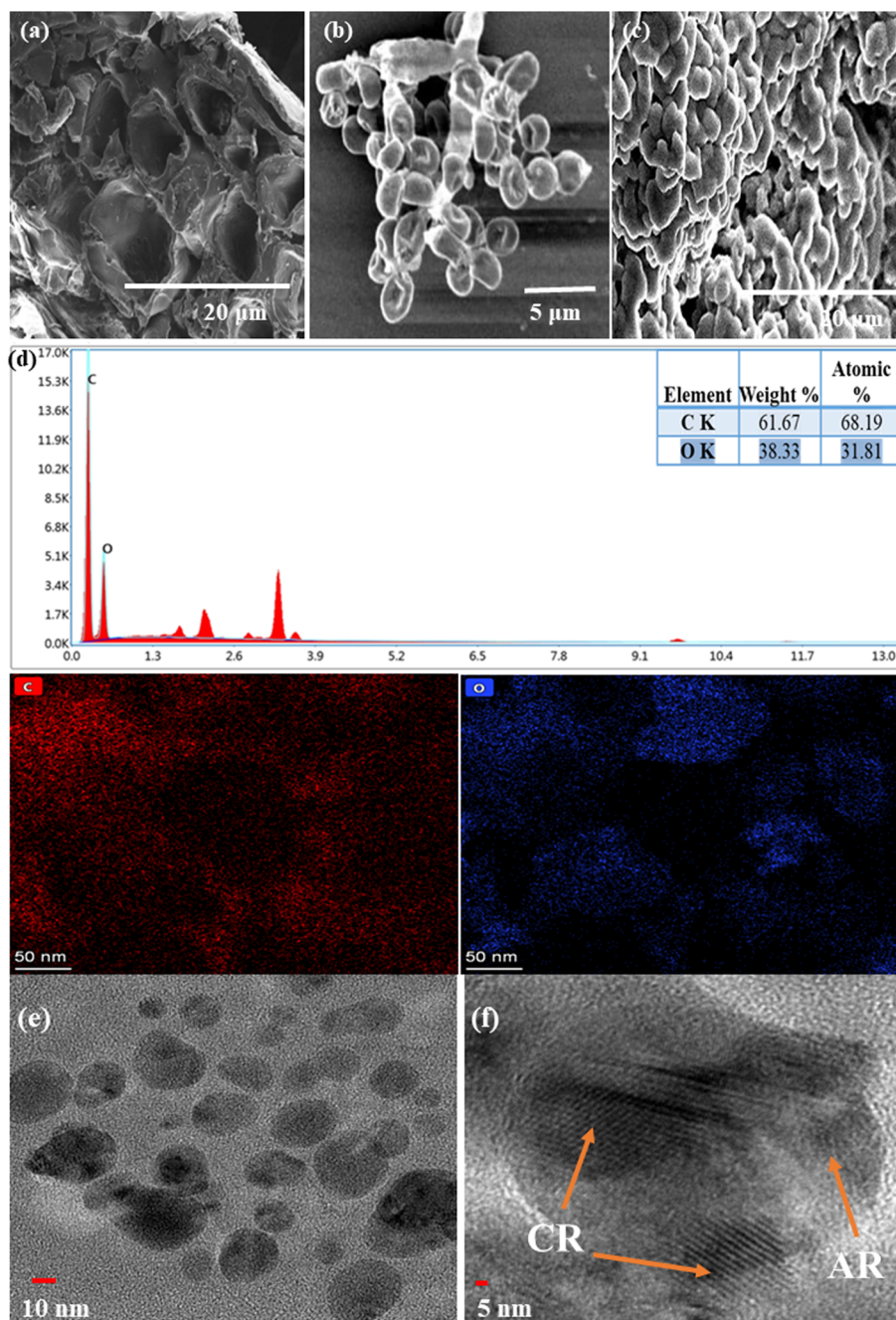**Fig. 4** (A) Thermal analysis of BEC and BCS and (B) DLS of BEC.

Fig. 5 FE-SEM micrographs of (a) BCS, (b) BEC, (c) BEC after adsorption with MG, and (d) EDAX of BEC with colour mapping of carbon and oxygen, (e and f) HRTEM images of BEC containing amorphous region (AR) and crystalline region (CR) respectively.

impacted by the pH of the dye solution.[36] Adsorption experiments of MG in the pH range of 2 to 8 were conducted to ascertain the impact of pH (Fig. 7a). In an aqueous solution, the protonated form of MG exists at a lower pH (pH ≤ 2.0) while the chromatic form is prevalent in the pH range of 2 to 8 and the carbinol form exists at pH > 8.0. As such, the variation of other parameters was carried out at pH ~ 6.0, above the pK_a value of MG (pK_a ~ 6.90), to prevent any colour changes resulting from the structural change of MG. As observed, MG uptake and removal percentage improved from 15.03 mg g^{-1} to 36.8 mg g^{-1}

and 37.59% to 92%, respectively, with an increase in the pH from 2.0 to 6.0. In the case of MG, which exists as a cationic entity at pH 6.0, forming a negative surface charge on cellulose at a greater pH promotes stable electrostatic bonding with MG molecules, resulting in enhanced MG sorption.

The influence of pH also corroborates the zeta potential results. From the zeta potential graph, the PZC value was determined to be at pH 3.8 (Fig. 7b), which suggests that the BEC composite has a predominance of negative charge on its surface as the pH of the solution exceeds the PZC value. The
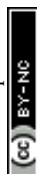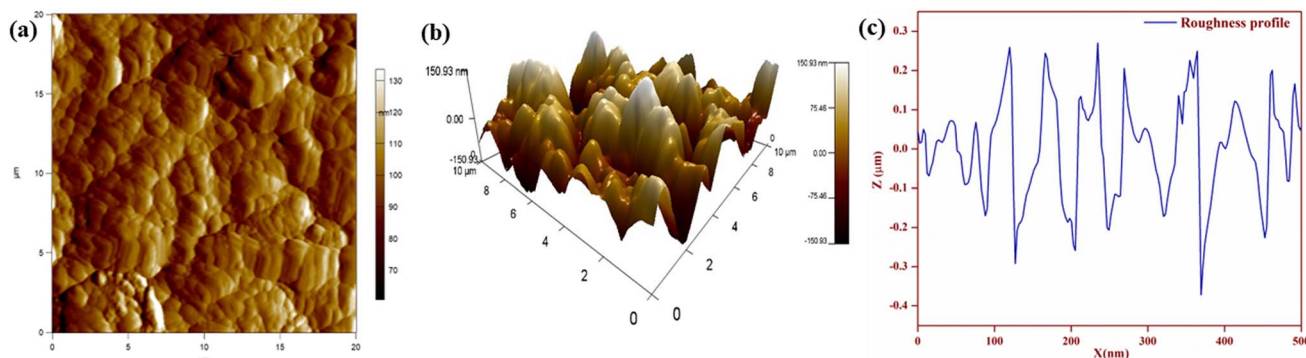
Fig. 6 AFM images of BEC (a) 2-D and (b) 3-D, and (c) roughness profile along the horizontal line drawn.
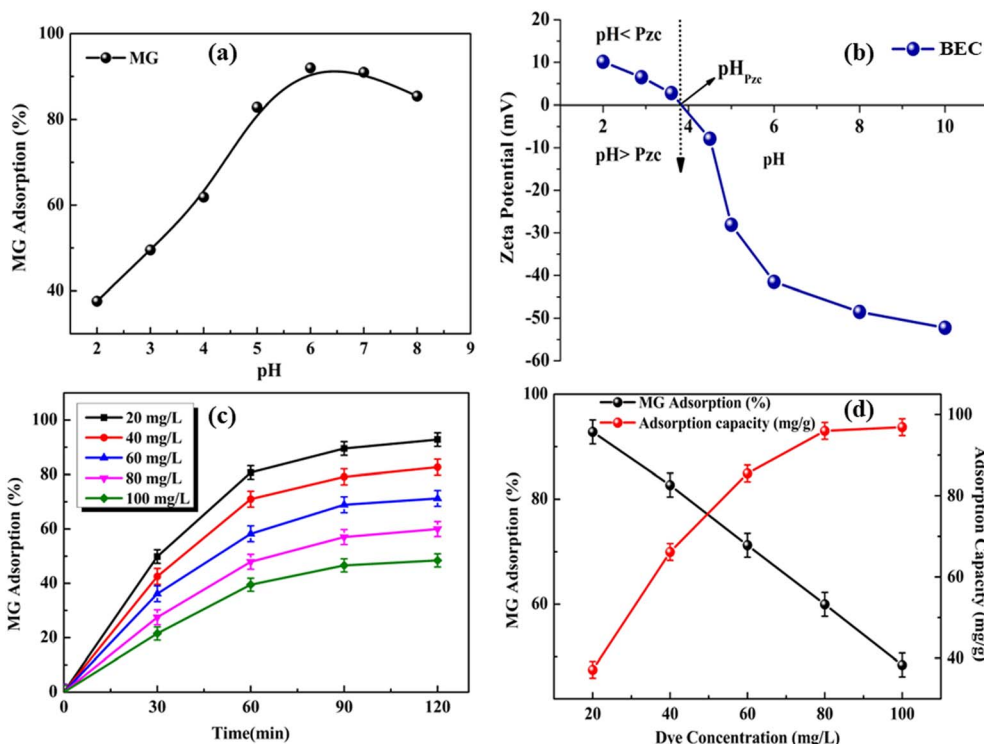

Fig. 7 (a) Effect of pH (adsorbent amount = 0.5 g L^{-1}; MG dye conc. = 20 mg L^{-1}; temperature = 25 °C), (b) pH_{pzc} of the BEC adsorbent, (c) effect of adsorption time, and (d) effect of dye concentration on MG dye removal by the BEC adsorbent (pH = 6; adsorbent amount = 0.5 g L^{-1}; contact time = 120 min; temp. = 25 °C).

general findings elucidate that the surface of the adsorbent carries a positive charge at pH values below the PZC, while at pH values above the PZC, it exhibits a negative charge. This property of the particles facilitates the removal of cationic dyes like MG from the solution utilizing the BEC adsorbent.[30] The optimum pH for the removal of MG was found to be at pH 6.0. Thus, the strong electrostatic force of attraction between the adsorbent and the dye is responsible for the greater removal efficacy at higher pH.[37,38]

3.8.2. Effect of contact time. The findings illustrated in Fig. 7c demonstrate the constant interaction between MG dye sorption behavior and contact time. The proportion of dye elimination increased as the interaction's temporal duration

was lengthened, and it finally reached equilibrium at 120 minutes. The adsorbent quickly adsorbed more than 70% of the dye during the first 60 minutes of contact, indicating an enhanced adsorption process. This initial rapid elimination rate can be ascribed to the large surface area that is initially accessible for the adsorption of dye moieties.[36]

As the initial concentration rises, the cellulose binding sites become saturated more quickly due to the increased competition among dye moieties. This leads to an insufficient number of active sites on the cellulose surface to accommodate the adsorbate, resulting in decreased removal efficiency. Conversely, when the initial dye concentration increases from 20 to 100 mg L^{-1}, it has a positive effect on adsorption capacity

(Fig. 7d). This occurs because the concentration gradient between the adsorbents and the aqueous solution increases with higher dye concentrations, enhancing the diffusion rate and promoting greater dye adsorption.

3.8.3. Adsorption isotherms. The adsorption isotherm study can be used to determine and suggest the distribution of the adsorbate. Isotherm parameters provide key insights into the adsorption mechanism, surface characteristics of the adsorbent, and the affinity between the adsorbate and adsorbent. The mechanism influencing the persistence or accessibility of a compound from aquatic porous surfaces or aquatic habitats to a solidified form at a constant temperature and pH is described by an adsorption isotherm.[39] Freundlich and Langmuir isotherm models were used to ascertain the applicability of adsorption as a technique for removing MG dye from aqueous solutions utilizing extracted cellulose.

The Langmuir isotherm model, which is successfully utilized in many single-layer adsorption processes, presumes that the sorption occurs at certain homogeneous sites on the adsorbent.[40,41]

The linear Langmuir equation can be stated in the form of:

$$\frac{C_e}{q_e} = \frac{1}{K_L} + \frac{a_L}{K_L C_e} \tag{5}$$

The non-linear Langmuir equation can be stated in the form of:

$$q_e = \frac{Q_{max} K_L C_e}{(1 + K_L C_e)} \tag{6}$$

where q_e (mg g^{-1}) and C_e are the optimum quantity of adsorbed dye and its remnant concentration. The Langmuir parameters are denoted as a_L (L mg^{-1}), while the optimum Langmuir intake potential is denoted as K_L (L g^{-1}).

In the Freundlich adsorption isotherm, heterogeneous multidimensional adsorption takes place between the adsorbate molecules because of the non-uniform energy distribution on the surface.[40,41]

The linear Freundlich equation can be stated as follows:

$$\log q_e = \log K_F + \frac{1}{n} \log C_e \tag{7}$$

The non-linear Freundlich equation can be stated as follows:

$$q_e = K_F C_e^{1/n} \tag{8}$$

where K_F and n denote the Freundlich coefficients for binding affinity and absorption ability.

The linear forms of the isotherm model were used to fit the optimal isotherm for the sorption of dyes on the sorbent molecule. In comparison to the Freundlich isotherm model ($R^2 \geq 0.94$), the Langmuir sorption isotherm model ($R^2 \geq 0.99$) has a greater correlation with the experimental data for the cellulose moiety. The findings indicated that the adsorption of dye molecules onto the BEC cellulose surface follows a monolayer process, with an adsorption capacity reaching 111.11 mg g^{-1}. The isotherms for MG dye were graphically illustrated, as shown in Fig. 8a and b (Table 2). This investigation demonstrates higher monolayer adsorption capacities compared to previously
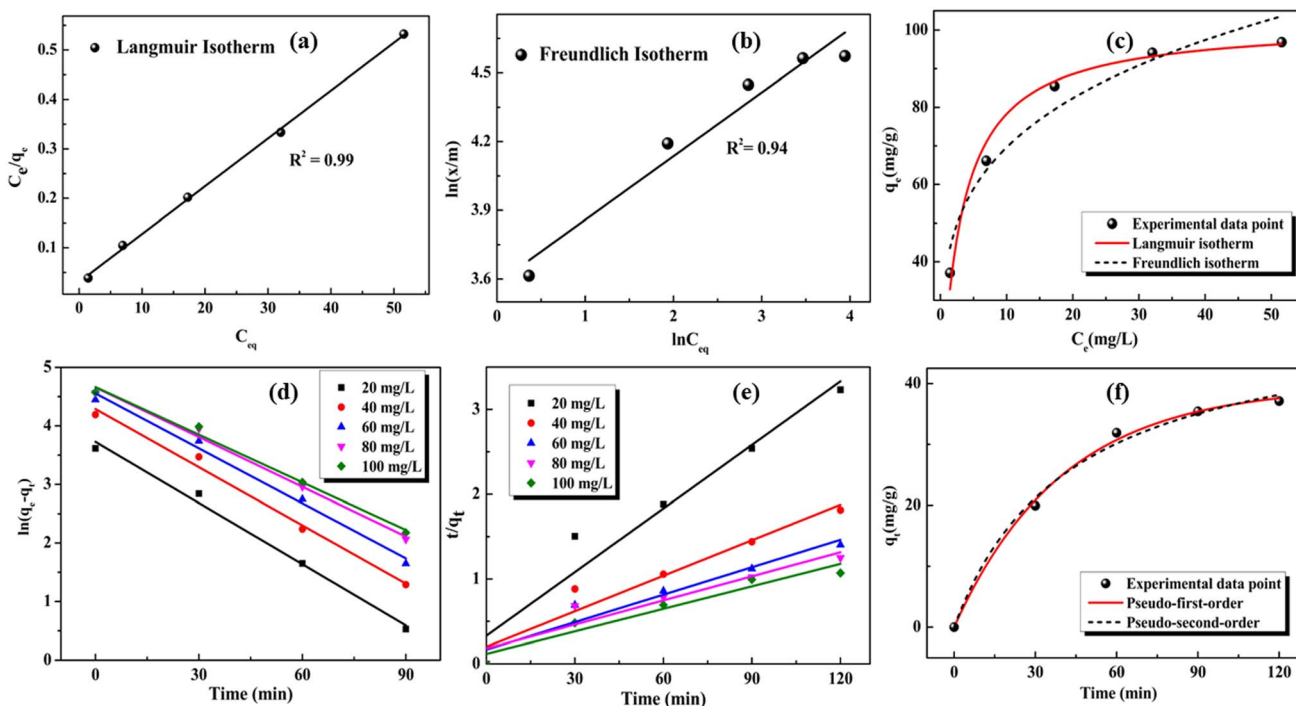

Fig. 8 At pH = 6 and an adsorbent amount of 0.5 g L^{-1}, the graph of (a) Langmuir and (b) Freundlich adsorption isotherms of MG. (c) Nonlinear fitting plots for both adsorption isotherms (d) pseudo-first-order kinetics, (e) pseudo-second-order kinetics of MG dye and (f) non-linear fitting plot for the kinetics of adsorption (temp. = 25 °C) for 20 mg per L MG dye solution.

Table 2 Adsorption isotherm parameters of the Langmuir and Freundlich models

Dye (MG)	Langmuir isotherm			Freundlich isotherm		
	Q_{max} (mg g^{-1})	K_L (L mg^{-1})	R^2	$1/n$	K_F (L mg^{-1})	R^2
	111.111	2.83	0.998	0.2707	0.2788	0.95

reported biosorbents. Examples include chitin from shrimp shell (malachite green: 38.21 mg g^{-1}),[42] neem sawdust (*Azadirachta indica*) (malachite green: 4.354 mg g^{-1}),[43] pineapple crown leaf (methyl violet: 31.24 mg g^{-1})[44] and princess tree leaf (Basic Red 46: 43.10 mg g^{-1}).[45]

To evaluate the best-fitting model for adsorption in nonlinear regression analysis of the adsorption isotherm, the chi-square (X^2) and Sum of Squared Error (SSE) values were computed. These values were estimated using the formulae provided below.

$$X^2 = \frac{(q_{e,exp} - q_{e,cal})^2}{q_{e,cal}} \quad (9)$$

$$X^2 = \frac{(q_{e,exp} - q_{e,cal})^2}{q_{e,exp}^2} \quad (10)$$

Here, $q_{e,cal}$ signifies the equilibrium dye uptake quantity, expressed in mg g^{-1}, as determined from the nonlinear plot. Conversely, $q_{e,exp}$ represents the equilibrium dye uptake amount obtained from experimental values. For the adsorption isotherm, the nonlinear regression analysis involved plotting q_e against C_e, as depicted in Fig. 8c. The Langmuir adsorption isotherm demonstrated a superior fit to the adsorption data, evidenced by its comparatively lower X^2 and SSE values (presented in Table S1).

3.8.4. Adsorption kinetics. The efficacy of the sorption process can be characterized by the sorption kinetics, which establishes the rate at which the sorbate is adsorbed on the surface of the sorbent moiety. The pseudo-first-order and pseudo-second-order kinetic models were used to assess the kinetics of MG sorption on the sorbent molecule. All the kinetics models stated above are expressed in linear form as follows:[46]

$$\ln(q_e - q_t) = \ln \quad q_e - k_1 t \quad (11)$$

$$\frac{t}{q_t} = \frac{1}{k_2 q_e^2} + \frac{1}{q_e} t \quad (12)$$

The non-linear form of the kinetic models is expressed as follows:

$$q_t = q_e(1 - e^{-k_1 t}) \quad (13)$$

$$q_t = \frac{q_e^2 k_2 t}{1 + k_2 q_e t} \quad (14)$$

The rate coefficients for the respective kinetic models, are designated by k_1 in min, and k_2 in g mg^{-1} min^{-1}. The quantity of dye sorbed per unit mass of cellulose is denoted by q_e and q_t (mg g^{-1}), respectively, at equilibrium and time t. C (mg g^{-1}) is the boundary thickness constant at time t. All the variables stated above are evaluated and provided in Table 3.

In the case of MG dye, the pseudo-second-order kinetic model's R^2 value is subpar (Fig. 8b). Additionally, there was a sizable difference in the residual sorption capacity (q_e) between the calculations and the experiment (Table 3), indicating that the second-order kinetics model experiment data were not suited well. The pseudo-first-order kinetics revealed that the kinetics data linearly fit with the sorption process, having $R^2 > 0.99$ for all initial MG dye concentrations. Since the results confirm that the sorption rates follow pseudo-first-order kinetics, the estimated q_e values for pseudo-first-order kinetics closely resemble those for MG (Fig. 8a).

The calculated q_e values increased as the initial amount of dye increased, and the rate constants shifted significantly, suggesting chemisorption, or the transfer and exchange of electrons between the absorbent and the substrate. At lower concentrations, there is less competition for sorption interface sites; hence the values of the rate constant k drop with the rise in the original dye concentration. Since there will be more competition for the interface-active sites at higher concentrations, lower adsorption rates will be observed.

Table 3 The determined parameters of pseudo-first-order and pseudo-second-order kinetic models for the adsorption of MG at different concentrations by BEC

MG (mg L^{-1})	$q_{e,exp}$ (mg g^{-1})	Pseudo first-order				Pseudo second-order		
		K_1	$q_{e,exp}$ (mg g^{-1})	R^2		K_2	$q_{e,exp}$ (mg g^{-1})	R^2
20	37.12	0.034	41.51	0.99		0.012	50.00	0.93
40	66.15	0.033	71.94	0.99		0.009	72.82	0.91
60	85.48	0.031	93.45	0.99		0.006	95.10	0.91
80	92.01	0.028	100.58	0.99		0.005	106.38	0.89
100	96.86	0.027	105.95	0.99		0.004	107.52	0.85

The aforementioned results also support the findings obtained from the non-linear regression analysis. To determine the kinetic model with the best fit, the X^2 and SSE values were calculated using eqn (7) and (8) and are presented in Table S2. The data indicate that the pseudo-first-order kinetic model provides the best fit, which is further evidenced by its lower X^2 and SSE values (Fig. 8f).

The mechanism and behaviour of adsorption are influenced by surface heterogeneity and interaction energy, while DFT simulations offer atomic-level insights into the energetics of adsorbate–surface interactions. The findings from the adsorption isotherm and kinetics model align with the DFT analysis. In the DFT analysis, a smaller ΔE_{GAP} value and strong binding energy suggest higher reactivity and a robust interaction between cellobiose and MG. The strong binding energy observed in the DFT analysis indicates a combination of physisorption and chemisorption interactions, which is consistent with the Langmuir isotherm and pseudo-first-order kinetics.

3.8.5. Thermodynamic parameter. Temperature is a crucial factor in the adsorption process. To assess its impact, batch adsorption experiments were performed at various temperatures (25, 35, and 45 °C) with an initial MG dye concentration of 20 ppm. The graph illustrates that as the temperature increases, the adsorption of MG dye also increases, indicating that the process is endothermic (Fig. S2a). This increase in the adsorbent's adsorption capacity is due to the higher energy available for interaction with dyes and the improved mobility of dye molecules.

The change in enthalpy (ΔH°) and entropy (ΔS°) in the adsorption process was calculated using the Van't Hoff equation (eqn (15)). The values of ΔH° and ΔS° were obtained from the slope and intercept of $\ln K_C$ vs. $(1/T)$ (Fig. S2b).[41]

$$\ln K_C = -\frac{\Delta H^\circ}{RT} + \frac{\Delta S^\circ}{R} \qquad (15)$$

$$K_C = \frac{q_e}{C_e} \qquad (16)$$

Here, K_C denotes the equilibrium constant, q_e (mg g^{-1}) and C_e (mg L^{-1}) signify the adsorbed dye quantity and the conc. of dye solution at equilibrium, T denotes the absolute temperature (K), and R is the universal gas constant. The negative ΔG° values decreased from -7.30 kJ mol^{-1} to -11.04 kJ mol^{-1} as the temperature increased from 298 K to 318 K, indicating that the adsorption process was feasible, spontaneous, and more favourable at elevated temperatures. Additionally, the ΔG° values of 0 and -20 kJ mol^{-1} suggest that the adsorption is a physisorption process.[47] The positive ΔH° value confirms the endothermic nature of the adsorption process, while the positive ΔS° value indicates an increase in randomness at the cellulose–MG interface (Table S3). Moreover, the positive ΔH° value suggested that the adsorption of MG by BEC was primarily driven by a chemisorption process. Therefore, based on the ΔG° and ΔH° values, it is likely that the adsorption of MG dye onto the BEC moiety involves both physisorption and chemisorption processes.[47,48]

3.8.6. Desorption and regeneration. The key to using adsorbents multiple times without a decline in adsorption capacity is recovery and regeneration. In Fig. 9a, the results of adsorption–desorption up to the fourth cycle are represented. As illustrated in the figure, there was an 8–10% reduction in MG adsorption in the fourth cycle, confirming the recyclable nature of cellulose and that the majority of adsorption occurs through chemisorption. This decline in adsorption percentage can primarily be attributed to the negligible loss of cellulose and retention of some adsorbed moieties on the cellulose surface. The results align with the FTIR spectra of MG adsorbed onto cellulose (Fig. 2A(c)). Peaks observed in the fingerprint region between 400 and 800 cm^{-1} are indicative of the mono and para-substituted benzene ring of the MG dye. This is further corroborated by the peak at 1595 cm^{-1}, which signifies the C–C stretching of the benzene ring in the MG dye.[31] The adsorption of the MG moiety on the cellulose surface leads to a decrease in adsorption efficiency after multiple cycles. Furthermore, the XRD pattern of the bare and adsorbed samples displayed no significant variations in the diffraction pattern, indicating the stability of the adsorbent, as shown in Fig. 9b.

3.8.7. Comparative assessment. The BEC adsorbent demonstrated superior and practical adsorption capabilities compared to traditional adsorbents like chitin, chitosan, and activated carbon composites. Although chitin and chitosan composites are biodegradable and effective at removing pollutants from wastewater, they need chemical modifications to improve their mechanical stability and adsorption efficiency.[42,50] Activated carbon is still considered the standard for
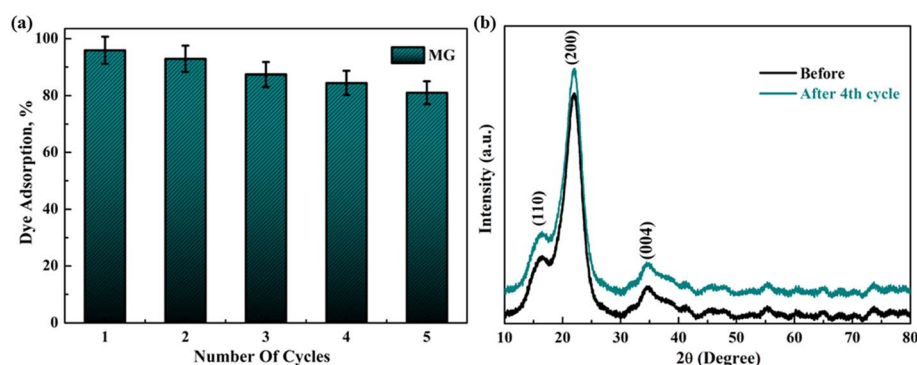

Fig. 9 (a) Recyclability and (b) XRD assessment of the adsorbent for the adsorption of malachite green.
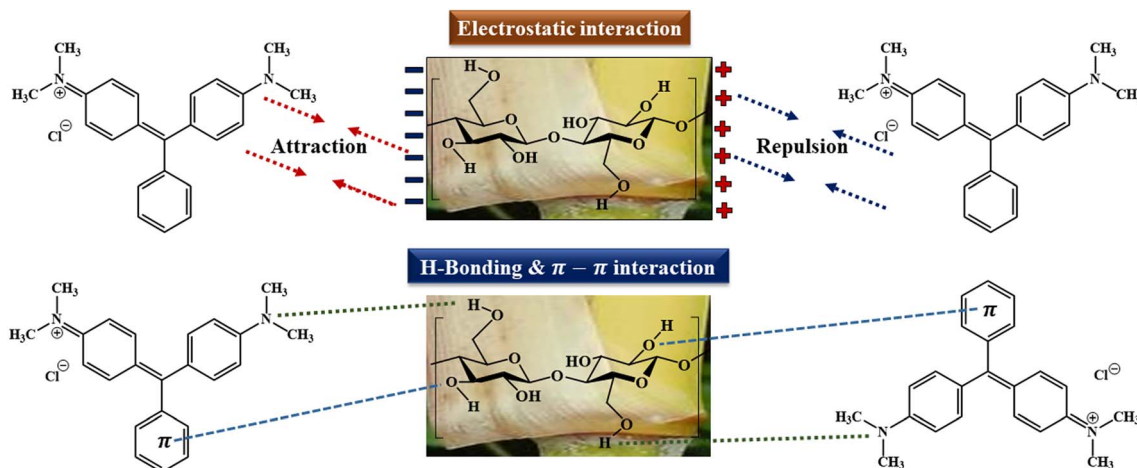
Fig. 10 Plausible adsorption mechanism of MG dye onto the BEC adsorbent.

high adsorption capacity due to its extensive surface area and porosity, but its high production costs and non-renewable nature hinder its sustainability.[20] In contrast, BCS cellulose showed similar adsorption efficiency while providing clear benefits in terms of renewability, cost-effectiveness, and environmental friendliness. Additionally, BCS cellulose maintained consistent performance across various pH levels and preserved its adsorption capacity after several regeneration cycles, underscoring its potential for practical applications. This study fills a significant gap in existing research by systematically evaluating a low-cost, sustainable, and regenerable adsorbent. By addressing the common performance-efficiency gap in bio-based materials, this work supports the development of next-generation green adsorbents designed for scalable water purification systems. Table S4 provides an overview of the sorption capacities of various sorbents under comparable experimental conditions.[40,42,49–54]

3.8.8. Plausible adsorption mechanism. A potential adsorption mechanism offers insights into the fundamental interactions and processes that govern this phenomenon (Fig. 10). The process involves the attachment of dye molecules to the surfaces of cellulose-based adsorbents, effectively extracting the dye from the solution. Experimental results indicate that MG dye removal was more efficient under alkaline conditions (solution pH > pH_{pzc}), highlighting the significance of electrostatic attraction in this process. The presence of additional peaks in FTIR analysis post-adsorption (Fig. 2A) further supports the role of electrostatic forces between pollutants and adsorbents. The bamboo culm sheath contains an ample amount of –OH groups, and after the MG adsorption, the transition of the –OH peak and the shifting of the functional groups in the FTIR spectra also provide evidence of hydrogen bonding and π–π interactions in the adsorption process.[3,16] In addition, the potential for hydrogen bonding between the hydroxyl group of the cellulose structure and the nitrogen atom in the MG molecule offers a plausible explanation for the observed greater adsorption affinity. The small ΔE_{GAP} value obtained from DFT analysis further supports this, as it indicates strong adsorption energies and stable interactions between the –OH groups and the amine moieties of MG. Notably, substantial MG adsorption occurred at high pH levels, suggesting that π–π interactions and hydrogen bonding may also play crucial roles alongside electrostatic interactions.[16] The nanostructure of the extracted cellulose component provides an extensive surface area for the physical adsorption of dye molecules. Adsorption isotherm and kinetics studies lend additional support to the proposed adsorption mechanism.

4 Conclusion

The study discovered that the cellulose extracted from BCS is an efficient and sustainable adsorbent for the removal of MG from aqueous solutions. Structural characterization using SEM confirmed the unique spherical, flat bowl-like morphology of BCS cellulose, while FTIR and DFT analyses identified functional groups that facilitated dye adsorption. The adsorption efficiency of BCS cellulose reached 92.8%, demonstrating rapid adsorption with minimal adsorbent usage. Isotherm modeling indicated that the Langmuir model (111.11 mg g^{-1}) provided the best fit, suggesting monolayer adsorption as the dominant mechanism. Additionally, kinetic studies confirmed that the pseudo-first-order model best described the adsorption process across all concentrations. These results establish BCS cellulose as a cost-effective and environmentally benign material for MG dye removal in wastewater treatment. Future studies should investigate its applicability for the removal of other pollutants and assess its feasibility for large-scale industrial applications.

Author contributions

Diptiranjan Behera: investigation, writing – original draft, visualization, conceptualization. Priyanka Priyadarsini Mishra: editing – original draft, formal analysis, methodology, visualization. Shruti Swaroop Pattnaik: methodology, supervision. Nigamananda Das: formal analysis, conceptualization, and characterizations. Jagadish Kumar: formal analysis, and

characterizations. Ajaya Kumar Behera: supervision, visualization, formal analysis, editing – original draft.

Conflicts of interest

There are no conflicts to declare.

Data availability

The authors declare that the data supporting the findings of this study are available in the paper.

Nonlinear kinetics plot of adsorption for different initial concentrations of MG dye (Fig. S1), the effect of temperature on the MG dye removal by BEC adsorbent, and $\ln K_C$ vs. $1/T$ plot to determine thermodynamic parameters for MG dye adsorption by BEC (Fig. S2), adsorption isotherm parameter for nonlinear regression analysis (Table S1), adsorption kinetics parameter for nonlinear regression analysis (Table S2), standard thermodynamic parameters for the adsorption of MG dye onto BEC (Table S3), comparative assessment of dye sorption processes (Table S4). See DOI: https://doi.org/10.1039/d5su00133a.

Acknowledgements

References

1 S. H. Azaman, A. Afandi, B. H. Hameed and A. M. Din, Removal of malachite green from aqueous phase using coconut shell activated carbon: adsorption, desorption, and reusability studies, J. Appl. Sci. Eng., 2018, 21(3), 317–330, DOI: 10.6180/jase.201809_21(3).0003.

2 C. Mohanty, N. Das, A. K. Behera and B. C. Tripathy, Efficiency of Poly(m-Aminophenol) as a Novel Adsorbent for Individual/Simultaneous Removal of Organic Dyes and Hexavalent Chromium from Water Sources, Water, Air, Soil Pollut., 2023, 234(3), 204, DOI: 10.1007/s11270-023-06221-y.

3 K. Ghosh, N. Bar, G. Roymahapatra, A. B. Biswas and S. K. Das, Adsorptive removal of toxic malachite green from its aqueous solution by Bambusa vulgaris leaves and its acid-treated form: DFT, MPR and GA modeling, J. Mol. Liq., 2022, 363, 119841, DOI: 10.1016/j.molliq.2022.119841.

4 C. Mohanty, P. P. Mishra, A. Samal, N. Das and A. K. Behera, Design of inexpensive, magnetically separable MnFe$_2$O$_4$/poly meta-amino phenol (PmAP) heterostructure: catalyst for bisphenol A & reactive blue 19 mineralisation, Environ. Sci.: Adv., 2024, 3(4), 561–571, DOI: 10.1039/D3VA00394A.

5 K. F. Kayani, Bimetallic metal–organic frameworks (BMOFs) for dye removal: a review, RSC Adv., 2024, 14(43), 31777–31796, DOI: 10.1039/D4RA06626J.

6 R. Fried, I. Oprea, K. Fleck and F. Rudroff, Biogenic colourants in the textile industry – a promising sustainable alternative to synthetic dyes, Green Chem., 2022, 24(1), 13–35, DOI: 10.1039/D1GC02968A.

7 V. Katheresan, J. Kansedo and S. Y. Lau, Efficiency of various recent wastewater dye removal methods: a review, J. Environ. Chem. Eng., 2018, 6(4), 4676–4697, DOI: 10.1016/j.jece.2018.06.060.

8 M. Zubair, S. Farooq, A. Hussain, S. Riaz and A. Ullah, A Review of Current Developments in Graphene Oxide-Polysulfone Derived Membranes for Water Remediation, Environ. Sci.: Adv., 2024, 3, 983–1003, DOI: 10.1039/D4VA00058G.

9 T. U. Rashid, S. F. Kabir, M. C. Biswas and M. R. Bhuiyan, Sustainable wastewater treatment via dye–surfactant interaction: a critical review, Ind. Eng. Chem. Res., 2020, 59(21), 9719–9745, DOI: 10.1021/acs.iecr.0c00676.

10 S. Biswas, A. K. Nayak and A. Pal, Surfactant-influenced biosorption as a sustainable and effective way for the eradication of environmental pollutants: a review, RSC Sustainability, 2025, 3, 112–133, DOI: 10.1039/D4SU00574K.

11 J. M. Antoniw, V. A. Gabriel, M. V. Kiriakou, M. A. Dubé, M. F. Cunningham and E. D. Cranston, Influence of cellulose nanocrystal surface chemistry and dispersion quality on latex nanocomposite stability, film formation and adhesive properties, RSC Appl. Polym., 2024, 2(2), 262–274, DOI: 10.1039/D3LP00244F.

12 N. Chandel, K. Jain, A. Jain, T. Raj, A. K. Patel, Y. H. Yang and S. K. Bhatia, The versatile world of cellulose-based materials in healthcare: from production to applications, Ind. Crops Prod., 2023, 201, 116929, DOI: 10.1016/j.indcrop.2023.116929.

13 S. Puri, S. Divakar, K. Pramoda, B. M. Praveen and M. Padaki, A Review on: Bio-inspired Nanoparticles and Its Impact on Membrane Application, RSC Sustainability, 2025, 3, 1212–1233, DOI: 10.1039/D4SU00460D.

14 M. Bassyouni, M. S. Zoromba, M. H. Abdel-Aziz and I. Mosly, Extraction of nanocellulose for eco-friendly biocomposite adsorbent for wastewater treatment, Polymers, 2022, 14(9), 1852, DOI: 10.3390/polym14091852.

15 S. Chauhan, P. Jamwal, G. S. Chauhan, K. Kumar, B. Kumari and S. Ranote, Tailoring of spherical nanocellulose via esterification with methionine followed by protonation to generate two different adsorbents for mercuric ions and Congo red, Int. J. Biol. Macromol., 2024, 279, 135313, DOI: 10.1016/j.ijbiomac.2024.135313.

16 Y. Y. Tan, A. A. Abdul Raman, M. I. I. Zainal Abidin and A. Buthiyappan, Sustainable Dye Adsorption Using Novel Activated Carbon Prepared from Passion Fruit (Passiflora edulis) Leaf: Mechanism and Cost Analysis, Ind. Eng. Chem. Res., 2023, 62(36), 14507–14521, DOI: 10.1021/acs.iecr.3c01303.

17 D. Behera, S. S. Pattnaik, D. Nanda, P. P. Mishra, S. Manna and A. K. Behera, A review on bamboo fiber reinforced composites and their potential applications, Emergent Mater., 2024, 1–16, DOI: 10.1007/s42247-024-00832-9.

18 S. Gu, A. Lourenço, X. Wei, J. Gominho, G. Wang and H. Cheng, Structural and Chemical Analysis of Three

Regions of Bamboo (Phyllostachys Edulis), *Materials*, 2024, **17**(20), 5027, DOI: 10.3390/ma17205027.

19 H. J. Al-Jaaf, N. S. Ali, S. M. Alardhi and T. M. Albayati, Implementing eggplant peels as an efficient bio-adsorbent for treatment of oily domestic wastewater, *Desalin. Water Treat.*, 2022, **245**, 226–237, DOI: 10.5004/dwt.2022.27986.

20 M. Mohammad and B. K. Dutta, Comparison of activated carbon and physic seed hull for the removal of malachite green dye from aqueous solution, *Water, Air, Soil Pollut.*, 2018, **229**(2), 45, DOI: 10.1007/s11270-018-3686-4.

21 G. Fan, M. Wang, C. Liao, T. Fang, J. Li and R. Zhou, Isolation of cellulose from rice straw and its conversion into cellulose acetate catalyzed by phosphotungstic acid, *Carbohydr. Polym.*, 2013, **94**(1), 71–76, DOI: 10.1016/j.carbpol.2013.01.073.

22 G. Yao, X. Zhu, M. Wang, Z. Qiu, T. Zhang and F. Qiu, Controlled fabrication of the biomass cellulose–CeO_2 nanocomposite membrane as efficient and recyclable adsorbents for fluoride removal, *Ind. Eng. Chem. Res.*, 2021, **60**(16), 5914–5923, DOI: 10.1021/acs.iecr.1c00012.

23 J. D. Hernández-Varela, J. J. Chanona-Pérez, H. A. C. Benavides, F. C. Sodi and M. Vicente-Flores, Effect of ball milling on cellulose nanoparticles structure obtained from garlic and agave waste, *Carbohydr. Polym.*, 2021, **255**, 117347, DOI: 10.1016/j.carbpol.2020.117347.

24 L. G. Bach, T. Van Tran, T. D. Nguyen, T. Van Pham and S. T. Do, Enhanced adsorption of methylene blue onto graphene oxide-doped XFe_2O_4 (X = Co, Mn, Ni) nanocomposites: kinetic, isothermal, thermodynamic and recyclability studies, *Res. Chem. Intermed.*, 2018, **44**, 1661–1687, DOI: 10.1007/s11164-017-3191-1.

25 F. Neese, Software update: the ORCA program system—Version 5.0, *Wiley Interdiscip. Rev.: Comput. Mol. Sci.*, 2022, **12**(5), e1606, DOI: 10.1002/wcms.1606.

26 I. A. Aguayo-Villarreal, D. Cortes-Arriagada, C. K. Rojas-Mayorga, K. Pineda-Urbina, R. Muñiz-Valencia and J. Gonzalez, Importance of the interaction adsorbent–adsorbate in the dyes adsorption process and DFT modeling, *J. Mol. Struct.*, 2020, **1203**, 127398, DOI: 10.1016/j.molstruc.2019.127398.

27 N. M. Praveena, P. Shaiju, R. A. Raj and E. B. Gowd, Infrared bands to distinguish amorphous, meso and crystalline phases of poly(lactide)s: crystallization and phase transition pathways of amorphous, meso and co-crystal phases of poly(L-lactide) in the heating process, *Polymers*, 2022, **240**, 124495, DOI: 10.1016/j.polymer.2021.124495.

28 M. S. Jahan, A. Saeed, Z. He and Y. Ni, Jute as raw material for the preparation of microcrystalline cellulose, *Cellulose*, 2011, **18**(2), 451–459, DOI: 10.1007/s10570-010-9481-z.

29 A. Kumar, Y. S. Negi, V. Choudhary and N. K. Bhardwaj, Characterization of Cellulose Nanocrystals Produced by Acid-Hydrolysis from Sugarcane Bagasse as Agro-Waste, *J. Mater. Phys. Chem.*, 2020, **2**(1), 1–8, DOI: 10.12691/jmpc-2-1-1.

30 N. F. Vasconcelos, J. P. A. Feitosa, F. M. P. Da Gama, J. P. S. Morais, F. K. Andrade, M. D. S. M. De Souza Filho and M. D. F. Rosa, Bacterial cellulose nanocrystals produced under different hydrolysis conditions: properties and morphological features, *Carbohydr. Polym.*, 2017, **155**, 425–431, DOI: 10.1016/j.carbpol.2016.08.090.

31 F. Jiang, D. M. Dinh and Y. L. Hsieh, Adsorption and desorption of cationic malachite green dye on cellulose nanofibril aerogels, *Carbohydr. Polym.*, 2017, **173**, 286–294, DOI: 10.1016/j.carbpol.2017.05.097.

32 M. Rasheed, M. Jawaid, B. Parveez, A. Zuriyati and A. Khan, Morphological, chemical and thermal analysis of cellulose nanocrystals extracted from bamboo fibre, *Int. J. Biol. Macromol.*, 2020, **160**, 183–191, DOI: 10.1016/j.ijbiomac.2020.05.170.

33 M. Rasheed, M. Jawaid, Z. Karim and L. C. Abdullah, Morphological, Physiochemical and Thermal Properties of Microcrystalline Cellulose (MCC) Extracted from Bamboo Fiber, *Molecules*, 2020, **25**(12), 2824, DOI: 10.3390/molecules25122824.

34 O. A. Oyewo, A. Adeniyi, B. B. Sithole and M. S. Onyango, Sawdust-based cellulose nanocrystals incorporated with ZnO nanoparticles as efficient adsorption media in the removal of methylene blue dye, *ACS Omega*, 2020, **5**(30), 18798–18807, DOI: 10.1021/acsomega.0c01924.

35 J. D. Hernández-Varela, J. J. Chanona-Pérez, H. A. C. Benavides, F. C. Sodi and M. Vicente-Flores, Effect of ball milling on cellulose nanoparticles structure obtained from garlic and agave waste, *Carbohydr. Polym.*, 2021, **255**, 117347, DOI: 10.1016/j.carbpol.2020.117347.

36 D. H. K. Reddy and S. M. Lee, Application of magnetic chitosan composites for the removal of toxic metal and dyes from aqueous solutions, *Adv. Colloid Interface Sci.*, 2013, **201–202**, 68–93, DOI: 10.1016/j.cis.2013.10.002.

37 M. Elhassan, M. R. R. Kooh, Y. F. Chou Chau and R. Abdullah, Hydrochar from Shorea spp.: a dual-purpose approach for sustainable biofuel and efficient methylene blue adsorbent, *Biomass Convers. Biorefin.*, 2025, **15**, 5779–5793, DOI: 10.1007/s13399-024-05376-w.

38 M. R. R. Kooh, M. K. Dahri and L. B. L. Lim, Removal of methyl violet 2B dye from aqueous solution using Nepenthes rafflesiana pitcher and leaves, *Appl. Water Sci.*, 2017, **7**, 3859–3868, DOI: 10.1007/s13201-017-0537-1.

39 G. Limousin, J. P. Gaudet, L. Charlet, S. Szenknect, V. Barthès and M. Krimissa, Sorption isotherms: a review on physical bases, modeling and measurement, *J. Appl. Geochem.*, 2007, **22**(2), 249–275, DOI: 10.1016/j.apgeochem.2006.09.010.

40 P. P. Mishra, P. Das, S. Paul, S. Manna, P. Basak, M. Das and A. K. Behera, Graphene oxide dots-loaded chitin flask a sustainable adsorbent for separating multiple dyes from water, *Environ. Qual. Manag.*, 2024, **34**(1), 1520–6483, DOI: 10.1002/tqem.22249.

41 S. S. Rath, N. Mohanty and B. N. Patra, Selective dye adsorption by pH modulation on chemically modified nanopolyaniline by N-grafting of maleic acid, *Polym. Chem.*, 2023, **14**(45), 5071–5082, DOI: 10.1039/D3PY00968H.

42 K. A. Kurnia, A. P. Rahayu, A. F. Islami, Y. Kusumawati, I. G. Wenten, A. U. Rahmah, D. V. Wellia and A. Saefumillah, Insight into the adsorption of dyes onto

chitin in aqueous solution: An experimental and computational study, *Arabian J. Chem.*, 2022, **15**(11), 104293, DOI: **10.1016/j.arabjc.2022.104293**.

43 S. D. Khattri and M. K. Singh, Removal of malachite green from dye wastewater using neem sawdust by adsorption, *J. Hazard. Mater.*, 2009, **167**(1–3), 1089–1094, DOI: **10.1016/j.jhazmat.2009.01.101**.

44 W. Astuti, T. Sulistyaningsih, E. Kusumastuti, G. Y. R. S. Thomas and R. Y. Kusnadi, Thermal conversion of pineapple crown leaf waste to magnetized activated carbon for dye removal, *Bioresour. Technol.*, 2019, **287**, 121426, DOI: **10.1016/j.biortech.2019.121426**.

45 F. Deniz and S. D. Saygideger, Removal of a hazardous azo dye (Basic Red 46) from aqueous solution by princess tree leaf, *Desalination*, 2011, **268**, 6–11, DOI: **10.1016/j.desal.2010.09.043**.

46 Y. Zhou, M. Zhang, X. Wang, Q. Huang, Y. Min, T. Ma and J. Niu, Removal of crystal violet by a novel cellulose-based adsorbent: comparison with native cellulose, *Ind. Eng. Chem. Res.*, 2014, **53**(13), 5498–5506, DOI: **10.1021/ie404135y**.

47 P. Arabkhani, A. Asfaram and M. Ateia, Easy-to-prepare graphene oxide/sodium montmorillonite polymer nanocomposite with enhanced adsorption performance, *J. Water Proc. Eng.*, 2020, **38**, 101651, DOI: **10.1016/j.jwpe.2020.101651**.

48 S. J. Peighambardoust, O. Aghamohammadi-Bavil, R. Foroutan and N. Arsalani, Removal of malachite green using carboxymethyl cellulose-g-polyacrylamide/montmorillonite nanocomposite hydrogel, *Int. J. Biol. Macromol.*, 2020, **159**, 1122–1131, DOI: **10.1016/j.ijbiomac.2020.05.093**.

49 A. C. Sadiq, N. Y. Rahim and F. B. M. Suah, Adsorption and desorption of malachite green by using chitosan-deep eutectic solvents beads, *Int. J. Biol. Macromol.*, 2020, **164**, 3965–3973, DOI: **10.1016/j.ijbiomac.2020.09.029**.

50 V. M. Muinde, J. M. Onyari, B. Wamalwa and J. N. Wabomba, Adsorption of malachite green dye from aqueous solutions using mesoporous chitosan–zinc oxide composite material, *J. Environ. Chem. Ecotoxicol.*, 2020, **2**, 115–125, DOI: **10.1016/j.enceco.2020.07.005**.

51 T. K. Arumugam, P. Krishnamoorthy, N. R. Rajagopalan, S. Nanthini and D. Vasudevan, Removal of malachite green from aqueous solutions using a modified chitosan composite, *Int. J. Biol. Macromol.*, 2019, **128**, 655–664, DOI: **10.1016/j.ijbiomac.2019.01.185**.

52 H. Tang, W. Zhou and L. Zhang, Adsorption isotherms and kinetics studies of malachite green on chitin hydrogels, *J. Hazard. Mater.*, 2012, **209**, 218–225, DOI: **10.1016/j.jhazmat.2012.01.010**.

53 M. Abewaa, A. Mengistu, T. Takele, J. Fito and T. Nkambule, Adsorptive removal of malachite green dye from aqueous solution using Rumex abyssinicus derived activated carbon, *Sci. Rep.*, 2023, **13**(1), 14701, DOI: **10.1038/s41598-023-41957-x**.

54 G. Y. Abate, A. N. Alene, A. T. Habte and D. M. Getahun, Adsorptive removal of malachite green dye from aqueous solution onto activated carbon of Catha edulis stem as a low cost bio-adsorbent, *Environ. Syst. Res.*, 2020, **9**, 1–13, DOI: **10.1186/s40068-020-00191-4**.